Victoria Shveytser[1], Paul C. Stoy[1,2,3], Brian Butterworth[4,5], Susanne Wiesner[1,2], Todd H. Skaggs[6], Bailey Murphy[2], Thomas Wutzler[7], Tarek S. El-Madany[7], Ankur R. Desai[2]

[1] Department of Biological Systems Engineering, University of Wisconsin – Madison.

[2] Department of Atmospheric and Oceanic Sciences, University of Wisconsin - Madison.

[3] Department of Forest and Wildlife Ecology, University of Wisconsin - Madison.

[4] Cooperative Institute for Research in Environmental Sciences, University of Colorado Boulder

[5] NOAA Physical Sciences Laboratory

[6] U.S. Salinity Laboratory, USDA-ARS

[7] Max-Planck Institute for Biogeochemistry, Jena, Germany

Corresponding author: Victoria Shveytser (shveytser@wisc.edu)

Key Points:

- Eddy covariance-measured evapotranspiration was partitioned to transpiration and evaporation using flux variance similarity at 12 sites
- Transpiration followed net radiation and was lowest in wetland ecosystems
- Daily evaporation varied little over time and amongst sites from summer to autumn
- Soil type determined the response of evaporation to large precipitation event

Abstract

Climate change is intensifying the hydrologic cycle and altering ecosystem function, including water flux to the atmosphere through evapotranspiration (ET). ET is made up of evaporation (E) via non-stomatal surfaces, and transpiration (T) through plant stomata which are impacted by global changes in different ways. E and T are difficult to measure independently at the ecosystem scale, especially across sites that represent different land use and land management strategies. To address this gap in understanding, we applied flux variance similarity to quantify how E and T differ across 12 different ecosystems measured using eddy covariance in a 10×10 km^2 area from the CHEESEHEAD19 experiment in northern Wisconsin, USA. The study sites included seven deciduous broadleaf forests, three evergreen needleleaf forests, and two wetlands. Net radiation explained on average 68% of the variance of half-hourly T, which decreased from summer to autumn. Average T/ET for the study period was 55% in forested sites and 46% in wetlands. Deciduous and evergreen forests

showed similar E trajectories over time despite differences in vegetation phenology. E increased dramatically after large precipitation events in loam soils but the response in sandy soils was more muted, consistent with the notion that lower infiltration rates temporarily enhance E. Results suggest that E and T partitioning methods are promising for comparing ecosystem hydrology across multiple sites to improve our process-based understanding of ecosystem water flux.

1 Introduction

Climate change is intensifying the water cycle and increasing extreme precipitation (Papalexiou & Montanari, 2019; Prein et al., 2017, Brutsaert, 2016; Eicker et al., 2016; Huntington, 2006). It is unclear if other critical parts of the global water cycle, like terrestrial evapotranspiration (ET), are decreasing in soil moisture (Jung et al., 2010), largely unchanging (Xue et al., 2020) despite increases in global atmospheric demand for water (Novick et al., 2016), or increasing due to global warming (Wang et al., 2022). ET moves some 65,500 km^3 of water into the atmosphere every year (Oki & Kanae, 2006) and is a central component of the global water cycle. It is critical to understand how the processes that comprise ET – transpiration (T) and evaporation (E) – respond to ongoing global changes the water cycle of a changing planet (Kool et al., 2014; Stoy et al., 2019).

T represents a biotic water flux to the atmosphere through plant stomata, while E comprises abiotic water flux pathways from the soil, plant surfaces, and other surfaces to the atmosphere. Both E and T are controlled by net radiation (Rn), vapor pressure deficit (VPD), air temperature (Ta), and atmospheric resistance as described by the Penman-Monteith equation (Monteith, 1965; Penman, 1948); but T is also driven also by vegetation properties, namely leaf area available for transpiration and canopy conductance which is influenced by the dynamic response of plant stomata to environmental cues. Plants respond to water scarcity by closing their stomata to save water while sacrificing carbon gain with considerable implications for carbon cycling. Stomatal closure also decreases evaporative cooling, which increases surface temperature and is therefore fundamental for understanding plant water stress and the atmospheric dynamics to which the land surface is coupled. Understanding how different ecosystems regulate water supplies reveals insight into how much water is available for groundwater recharge and runoff (Anderson et al., 2017), and how ecosystem management decisions impact water cycling.

E and T can be measured using lysimeters, leaf-level gas exchange measurements, sap flow, and more (Kool et al., 2014), but are difficult to scale up to the ecosystem level (Berkelhammer et al., 2016). Ecosystem ET, is readily measured using eddy covariance, but most studies do not seek to partition eddy covariance measured-ET into its components, which results in a paucity of ecosystem-scale E and T observations to understand the impacts of land use and land management changes on water cycling (Stoy et al., 2019). Water balance (Liu et al., 2016), machine learning (Granata et al., 2020), remote sensing (Martens et al.

2017), land surface models and hydrologic models (Sun et al., 2017; X.-J. Zhang et al., 2014) can all be used to help estimate the contributions of E and T to ET at different spatial and temporal resolutions, but often rely on assumptions that require further validation. A large contributor to our uncertainty in understanding ET across multiple scales is the lack of ground based E and T observations at the ecosystem scale (Rigden et al., 2018).

Most eddy covariance studies focus on a single ecosystem, paired ecosystems in close proximity, or multiple ecosystems across large spatial extents, few have measured multiple ecosystems in close proximity, which is critical for understanding how different ecosystems contribute to the water balance of heterogeneous landscapes (Sun et al., 2021; Chu et al. 2021). We seek to address this by estimating E and T directly at the ecosystem scale at multiple sites within a diverse landscape using a dense array of eddy covariance towers within a 10 $\times$ 10 km^2 area (Butterworth et al., 2021). We do so using an approach developed to partition carbon and water fluxes from high frequency eddy covariance measurements called flux variance similarity (FVS) (Scanlon & Kustas, 2012; Scanlon & Sahu, 2008). FVS assumes that stomatal and non-stomatal fluxes independently conform to Monin-Obukhov similarity theory and has been successfully applied to study E and T across multiple global ecosystems (Kustas et al., 2018; Perez-Priego et al., 2018; Rana et al., 2018; Scanlon & Kustas, 2012; Sulman et al., 2018; Wagle et al., 2020) but less frequently in forests and wetlands (Klosterhalfen et al., 2019; Sulman et al., 2018), leaving opportunities for understanding the pathways by which different ecosystems use water.

Here, we use FVS to directly partition E and T from ET measurements across multiple forest and wetland ecosystems in northern Wisconsin, USA. We briefly describe the study ecosystems and their relationship with conditions that result in successful partitioning of the FVS algorithm. We focus our analysis on quantifying the response of E and T from the study ecosystems to the diverse climatic conditions and phenological changes experienced during the measurement period across the transition from summer to autumn. We hypothesize that i) the wetlands and forested sites will partition E and T differently across the study period and that wetlands will support more E. More specifically, we expect that ii) T will dominate ET during summer due to high energy inputs and leaf area and E will dominate ET during autumn in the forested ecosystems due to decreased T, and that iii) T will differ little amongst forest ecosystems following the notion that it is a "conservative" quantity that is relatively insensitive to forest type (Oishi et al., 2010; Roberts, 1983).

2 Materials and Methods

2.1 Study Sites

The Chequamegon Heterogeneous Ecosystem Energy-balance Study Enabled by a High-density Extensive Array of Detectors 2019 (CHEESEHEAD19) was designed to understand how the atmospheric boundary layer responds to heterogeneity in land surface structure and function (Butterworth et al., 2021). It

deployed one of the highest density networks of eddy covariance measurements of surface-atmosphere energy fluxes to date: 19 flux towers in a 10 × 10 km^2 area among an extensive array of land surface and atmospheric measurements in northern Wisconsin, USA, centered around the existing 447-m WLEF tower AmeriFlux site (US-PFa) (45.9459, −90.2723) (Figure 1, Table 1) near Park Falls, Wisconsin USA. This region is located in the Köppen climate zone: Dfb: warm-summer humid continental (Beck et al., 2018). The July - October 2019 measurement period allowed us to capture how seasonal changes in vegetation structure and function impact E and T. Mean annual temperature is 4.33 °C and mean annual precipitation is 823 mm with significant precipitation in all seasons.

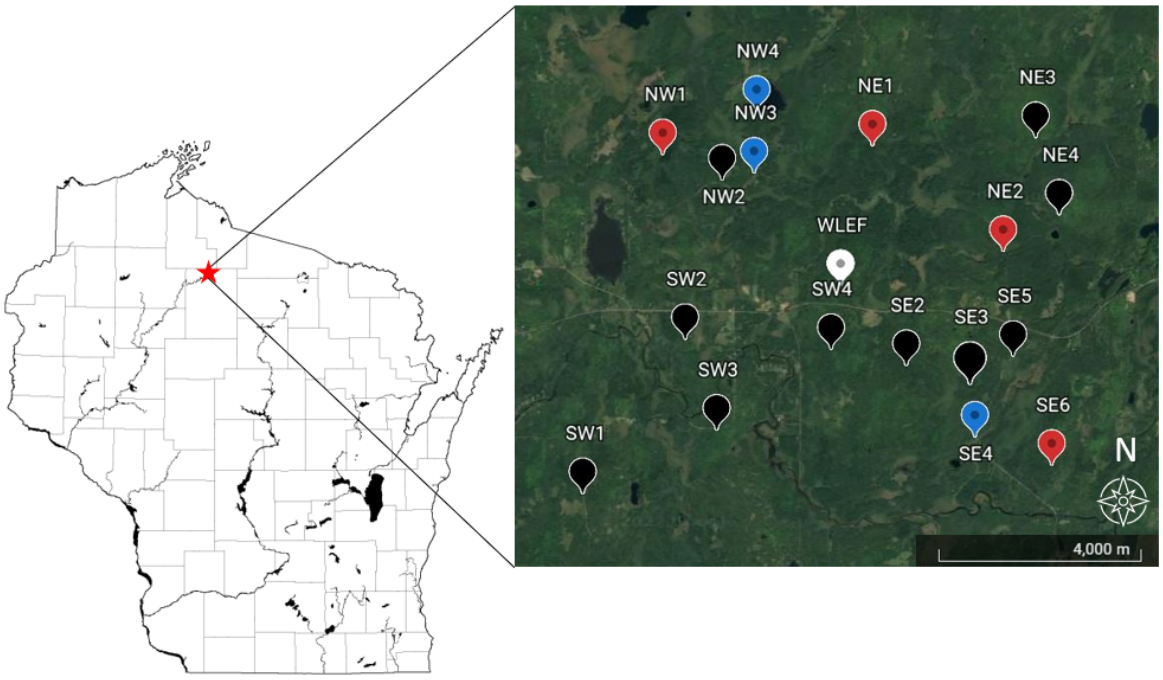

Figure 1. A map of 17 of the CHEESEHEAD19 eddy covariance study sites in a 10 × 10 km^2 area in northern Wisconsin, USA. Sites are labeled with abbreviations used in the CHEESEHEAD19 project (Butterworth et al., 2021) (Table 1). Black indicates deciduous broadleaf sites, red indicates evergreen needleleaf sites, blue indicates wetland sites, and white indicated the WLEF tower. (Google Earth & Wisconsin State Cartographer's Office, 2022)

Tower placement within the study domain followed a stratified random grid pattern with towers placed on average 1.4 km away from their nearest neighboring tower and 3.5 km from the WLEF tall tower (Davis et al., 2003; Xu et al., 2017). This partial randomization – taking distance to road, USFS-owned land and appropriate tree gap for tower into consideration – resulted in spatial variability in

vegetation height and ecosystem type including observations in challenging flux measurement conditions. The study ecosystems included four evergreen needleleaf forests (ENF) sites dominated by *Pinus spp., Picea mariana* and/or *Larix spp.*, two wetland sites (WET), four aspen (*Populus tremuloides)*- dominated sites, one maple (*Acer saccharum)*-dominated site, and five mixed forest sites, one of which was near a lake, and most of which are a mix of aspens and pines (Table S1). All mixed and deciduous forests are denoted as deciduous broadleaf forests (DBF) for the purposes of this study given that their change in leaf area across the seasonal transition will differ from ENF sites. Towers were mounted 32 m above ground level at the forest sites and between 1-3 m above ground level at the wetland sites (Table 1). Of the 19 EC towers, 17 used an open path infrared gas analyzer rather than closed path systems to which an additional density term needs to be applied to the Fluxpart algorithm (Stoy et al., 2019), described below. Of these 17 sites, we study 12 due to data availability but provide an extended description of all in Table S1.

The study towers were part of the Integrated Surface Flux System (UCAR/NCAR) and included CSAT3 sonic anemometers and EC150 open-path infrared H_2O/CO_2 gas analyzers (Campbell Scientific, Inc) to measure turbulent fluxes, a NR01 four-component radiometer (Hukseflux, Delft, The Netherlands), and SHT85 aspirated air temperature (Ta) and relative humidity (RH) sensors (NCAR) above the plant canopies VPD was calculated. Ta and RH were also measured at 2 m and at mid-canopy in the forests. Soil measurements included four-level soil temperature measurements (NCAR) at 0.6, 1.9, 3.1, and 4.4 cm depths, EC-5 soil moisture probes (Decagon, Pullman, WA) at 5 cm, and HFT heat flux plates at 5 cm in forested sites and buried in mats in the wetlands. Precipitation was measured at a SURFRAD station, a ground-based measurement system for continuous long-term measurements of climatic data, located at a grass field within the CHEESEHEAD19 study domain at 45.9458, −90.2944.

2.2 Eddy Covariance and Flux Partitioning

The eddy covariance (EC) method is widely used to measure carbon dioxide and water vapor fluxes worldwide (Baldocchi, 2014). Eddy covariance takes high-frequency (10–20 Hz) measurements of three-dimensional wind velocity, CO_2, and H_2O concentrations in the roughness sublayer over the plant canopy. Assuming that turbulent mixing is sufficient, half-hourly (or hourly) net ecosystem-scale flux measurements can be calculated. However, to improve our process-level understanding of ecosystems and to improve models, EC fluxes need to be partitioned into their separate parts: photosynthesis and respiration for carbon dioxide fluxes and E and T for water. This underlies the need for effective and accurate flux partitioning methods (Kool et al., 2014; Stoy et al., 2019).

A promising approach for partitioning ET into T and E is flux-variance similarity (FVS) (Scanlon & Kustas, 2010). FVS assumes that stomatal and non-stomatal turbulent fluxes conform independently to Monin-Obukhov Similarity Theory. For a brief conceptual description, assume that there are two end-member scenar-

ios for a parcel of air transported from the surface: one that interacts only with stomata and one that does not. An eddy transported away from a surface that is respiring CO_2 and evaporating water through pathways other than stomata will have deviations from mean CO_2 concentration (c') and water vapor concentration (q') that are positively correlated. An eddy of air that interacts with a surface with open stomata will have a negative relationship between c' and q' that is determined by plant water use efficiency (WUE) with more water vapor and less carbon dioxide (due to photosynthesis) than surrounding air. WUE can be used to establish a relationship between the variance of CO_2 associated with stomatal intake and the correlation between stomatal and non-stomatal CO_2 exchange processes (Figure 2).

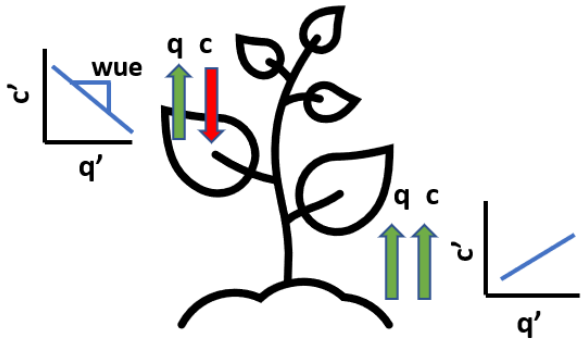

Figure 2. A schematic representation of basics of flux variance and correlation between stomatal and non-stomatal CO_2 and water vapor exchange processes.

In this way, evapotranspiration (ET) can be partitioned into E and T by matching observed correlations of q' and c' that represent a combination of stomatal and non-stomatal processes to those that correspond to purely stomatal or non-stomatal processes (Scanlon & Sahu, 2008). Subsequent work by Skaggs et al. (2018) noted an algebraic solution to terms that had previously been solved numerically (Palatella et al., 2014). The analytical solution was incorporated into an open-source Python 3 module, Fluxpart (Skaggs et al. 2018), that implements the FVS method to partition E and T. The original FVS approach of Scanlon et al. (2010) used a simple WUE formulation, which assumes a constant ratio between leaf-internal CO_2 concentrations and atmospheric CO_2 concentration of 0.7 for C3 plants following Campbell and Norman (1998). Fluxpart also implements other methods for WUE, including models in which intercellular CO_2 varies as a function of VPD (Skaggs et al., 2018), and a model in which optimal stomatal behavior is assumed in response to VPD (Scanlon et al., 2019). We compared the constant ratio and optimality models and chose the constant ratio approach because it had a greater amount of successfully partitioned measurements (see Table S8). Fluxpart also applies quality control routines to the high-frequency data, correcting for external fluctuations associated with air temperature and vapor density (Detto & Katul, 2007; Webb et al., 1980).

Fluxpart delivers predictions of latent heat flux due to evaporation (LEe) and transpiration (LEt) from the eddy covariance latent heat flux measurements (LE) with units of W m^{-2}. E, T, and ET in mm half $hour^{-1}$ were calculated by dividing their corresponding LE by the latent heat of vaporization using the equation of Henderson-Sellers (1984) and the density of water. It is important to note that the Fluxpart algorithm is not always able to make the calculation for different reasons. FVS and the eddy covariance methodology assume the surface-atmosphere exchange is well-represented by a turbulent flux, which is not always the case, especially at night (Zhu et al., 2006). Additionally, the FVS method is applicable only when a negative carbon flux exists due to photosynthesis, and positive carbon and water fluxes exist due to respiration, transpiration and evaporation, and when eddy covariance measured fluxes, variances, and correlations for CO_2 and water satisfy several constraints (Scanlon et al., 2019, Eq 13). FVS results tend to match known fluxes generated using large eddy simulation when there is a clear separation of CO_2 and H_2O sinks and sources (Klosterhalfen et al., 2019). As a consequence of these limitations and the fact that eddy covariance time series contain multiple gaps (e.g. due to weather or instrumentation, etc.), we gap filled missing E, T, and ET data to create continuous time series over the study period.

Eddy covariance data were gap filled using REddyProc (Wutzler et al., 2018) for R (R Core Team, 2021). REddyProc inputs half-hourly eddy covariance data and performs quality checks and data filtering based on measured flux and friction velocity to discard data collected under insufficient turbulence. LE was gap filled using a mean diurnal course algorithm, which replaces missing values based on observations measured within one hour of adjacent days if climate conditions are similar. We also used this algorithm to gap fill FVS-generated LE due to evaporation (LEe) and transpiration (LEt) – which were converted to E and T – under the assumption that these fluxes, like ET, vary little from day to day with similar climate forcing.

We analyzed the success rate of FVS partitioning to site and measurement characteristics using linear regression to explore if there were certain circumstances that led to greater partitioning success. Partitioning success was analyzed against LAI, canopy (z) and instrument height (h), the distance between them (z-h) and the ratio between them (z/h). We also used linear regression to explore the effects of abiotic factors on E and T, namely their response to net radiation following the Priestley Taylor equation (Priestley & Taylor, 1972) which assumes that water fluxes follow linear response to net radiation when water is not limiting.

2.4 Uncertainty analysis

Eddy covariance measurements, like all measurements, contain uncertainty, which must be quantified for a robust estimate of net fluxes (Goulden et al., 1996). We used the approach of Richardson et al. (2006) which assumes that surface-atmosphere fluxes taken under similar climatic conditions at the same time on consecutive days should be approximately equal, and thereby uses dif-

ferences between these measurements to estimate a random error, which trends to follow a Laplacian (double exponential) distribution (Hollinger & Richardson, 2005). We performed a sensitivity analysis on the conditions considered to be sufficiently similar by Richardson et al. (2006) – photosynthetic photon flux density differences less than 37.5 µmol m^{-2} s^{-1}, air temperature differences less than 3 °C , and wind speed differences less than 1 m s^{-1} – and found little justification to use other values. We added a wind direction threshold of a difference of no greater than 30 degrees to account for heterogeneous vegetation surrounding some towers. We then used this "daily differencing" approach to calculate the standard deviation of measured or FVS-partitioned ET, T, and E by calculating the linear relationship between the magnitude of the flux and its standard deviation, and applying this linear model to all observations, which was taken to be the random error of the measurements.

Gap filling uncertainty was calculated using the standard deviation of the marginal distribution sampling calculated by REddyProc output (Wutzler et al., 2018) for ET, T, and E. We combined gap filling uncertainty for the gap filled quantities with random uncertainties of the measurements to create a continuous vector of the standard deviation of ET, T, and E at half-hourly time intervals. The resulting standard deviation estimates were autocorrelated, and uncertainty was propagated by estimating the effective number of observations after accounting for autocorrelation (nEff) using 'lognorm::computeEffectiveAutoCorr' (Wutzler 2021) in R. We used the observed and gap filled flux measurements to compute nEff because the magnitude of measurement uncertainty is a function of the magnitude of the flux (Richardson et al. 2006), and because this approach provided a more conservative estimate of the standard error of the mean flux value. We computed the standard error of the mean for each latent heat flux (LEe, LEt, and LE) for each ecosystem for which sufficient partitioned values were obtained (described further in Section 3), by first calculating the variance for random and gap filling uncertainty (x) separately using

$$Var(x) = \frac{\overline{\sigma_x^2}}{nEff-1} \quad (1)$$

Where $\overline{\sigma_x^2}$ is the mean value of the variance that describes the random or gapfilling uncertainty of each flux (LEe, LEt, and LE). The total standard deviation was then calculated by summing variances. Significant differences in the mean value for each site were calculated using one-way ANOVA with Tukey's HSD post-hoc test. The Bonferroni filter was applied to adjust the 95% significance level for the 66 comparisons that resulted from analyzing differences amongst 12 sites: $(1-0.95)/66 = 0.00076$.

2.5 Visualization

We are faced with the challenge of presenting time series observations from multiple ecosystems in response to similar environmental drivers. Throughout, we use a Butterworth filter (Butterworth, 1930) to smooth micrometeorological, eddy covariance, and FVS-generated time series as a visual aid, taking advan-

tages of the filter's ability to exclude high frequencies that complicate visual representation while being uniformly sensitive to the lower frequencies that display the dominant patterns in the time series. The measurement record at three of the sites began in late July while the rest began in early July, which complicated the visual presentation; we simply excluded these sites from the figures to aid readability. All statistical analyses are applied to the raw and not the filtered data.

3 Results

Rn (Figure 3A) and Ta (Figure 3B) decreased from summer to autumn with oscillations at approximately weekly time scales as a consequence of synoptic-scale meteorological drivers observed during the measurement period (Desai et al., 2021). A maximum temperature of 27.7 °C was observed on July 5 with a minimum of 2.3 °C on October 5. There was an extended period of above-average temperatures for over a week beginning September 16; such positive temperature anomalies during autumn are a common feature of the climate of the Upper Midwest. The temperature difference between the top of the canopy and the bottom of the canopy decreased throughout the season (not shown) suggesting more energy reaching the ground as leaves begin to fall despite decreasing Rn throughout the seasonal shift.

A pluvial growing season was experienced in 2019 with frequent rain events across the entire measurement period (Figure 4a): Precipitation across the State of Wisconsin deviated from average by a positive 39.1 mm in July, negative 6.1 mm in August, positive 83.3 mm in September, and positive 63.5 mm in October (NOAA 2022). The average daily precipitation event was 8.34 mm/day, excluding trace rainfall, with a maximum event of 52 mm on September 3. The longest period without a rain event was 8 days in late-August. Soil moisture at most sites it dropped to its lowest point in late-August at the end of the period without rain (Figure 4b and Figure S1). The highest soil moisture content followed the large storm event in September, peaking on September 13 (Figure 4b). The one-dimensional water balance (the cumulative sum of precipitation minus evaporation for the study period) reached a positive water balance during the measurement period in early September (Figure 4c) during the large precipitation events at most sites. Atmospheric VPD was similar among the forested ecosystems where it averaged (3.47 kPa) but was lower in the wetland ecosystems (1.32 kPa) (Figure 4d).

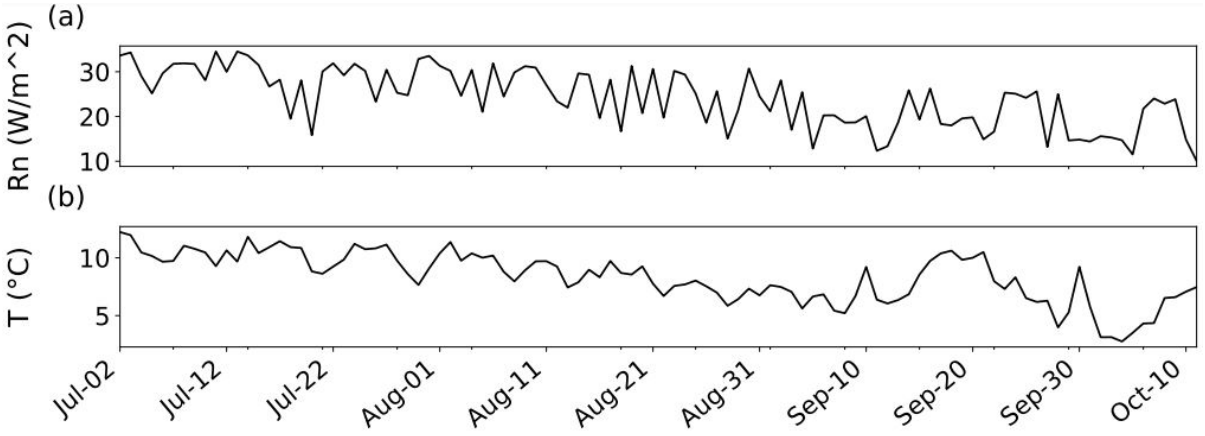

Figure 3. The daily average of thermodynamic variables (a) net radiation and (b) air temperature for a representative tower, NE2 (Figure 1, Table 1) during the 2019 measurement period.

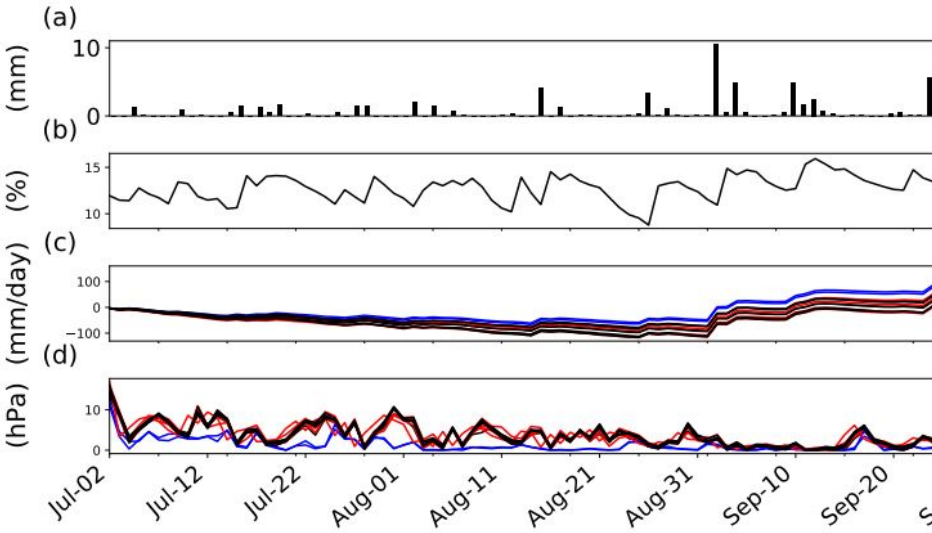

Figure 4. Hydrological variables during the July mid-October 2019 measurement period. (a) Precipitation measured at the SURFRAD station, (b), soil water content for a representative site, NE2 (Table 1) (See Figure S1 for more sites), (c) the one-dimensional water balance at all sites (cumulative sum of evapotranspiration subtracted from cumulative sum of precipitation), and (d) daily averaged vapor pressure deficit. ENF sites are denoted in red, DBF sites in black, and wetlands in blue.

3.2 FVS Partitioning

The FVS algorithm was satisfied the constraints of physically realistic solutions 41% of the time at SE6, an ENF site (Table 2), but never did at NE1 and

satisfied these constraints less than 25% of the time at NW2, SW2, SE4, and SE5. These sites were removed from subsequent analyses with the exception of the wetland site SE4 (with $>$ 20% partitioning success) which was left in the interest of comparison against other wetland sites. NE3 was also left out of analysis, despite higher success, due to late start of data in mid-July. This left 12 sites for the subsequent analyses for which FVS resulted in a physically realistic solution between 26 to 41% of the time. The lack of partitioning for most sites is due mainly to missing data in some capacity, which accounted for between 15% and 42% of invalid partitioning data, depending on the site. The rest of the errors (Table 2) were largely due to an inability to satisfy realistic solutions and error messages indicating that the observation did not align with Monin-Obukhov similarity theory. Partitioning success increased with a greater difference between instrument height and canopy height (R^2 = 0.30), but no relationship between partitioning and position of measurements relative to the roughness sublayer (using instrument height to canopy height ratio as a proxy) was found, nor between partitioning success and LAI, instrument height, or canopy height.

3.3 Evapotranspiration

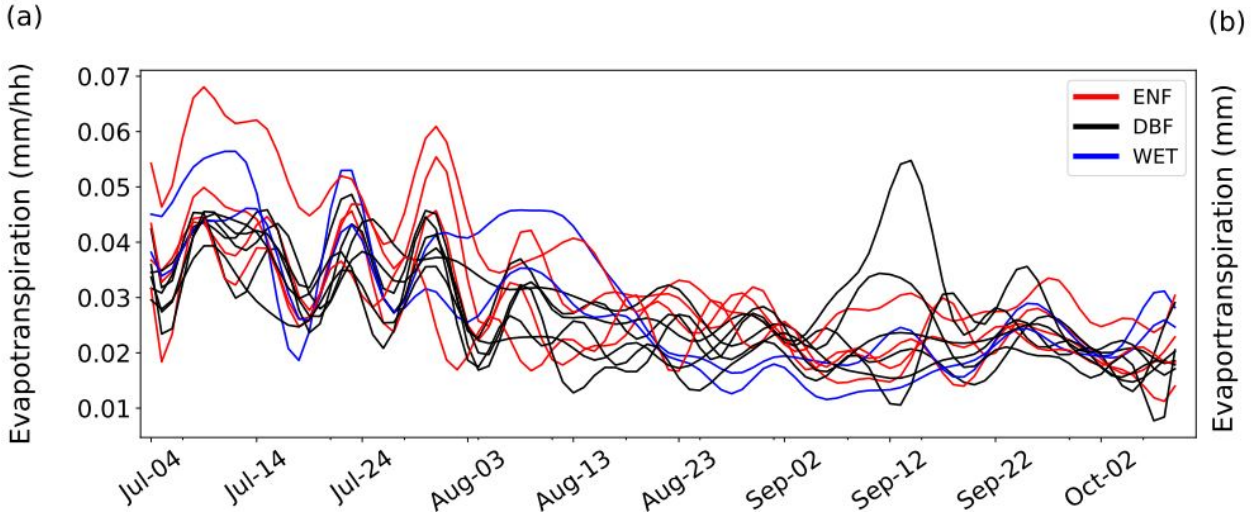

Figure 5. (a) The daily median evapotranspiration (ET) from July 3rd to October 11th, 2019, for all sites smoothed with a Butterworth filter to aid visualization, and (b) the cumulative sum of evapotranspiration across all sites. ENF sites are denoted in red, DBF sites in black, and wetlands in blue.

ET generally decreased from summer to fall (Figure 5a), in response to fluctuations in Rn at approximately weekly time scales that correspond to frontal weather systems (Figure 3a). The ET (as well as E and T) uncertainty analysis indicated that cumulative fluxes from most sites were significantly different from most other sites (Table S2), but there was no difference amongst forests

dominated by DBF or ENF trees (Figure 5) when comparing cumulative sums. Wetland sites had significantly lower average ET over the measurement period (244 mm), than forested sites (307 mm) (P<0.0001, Figure 5b).

3.4 Evaporation

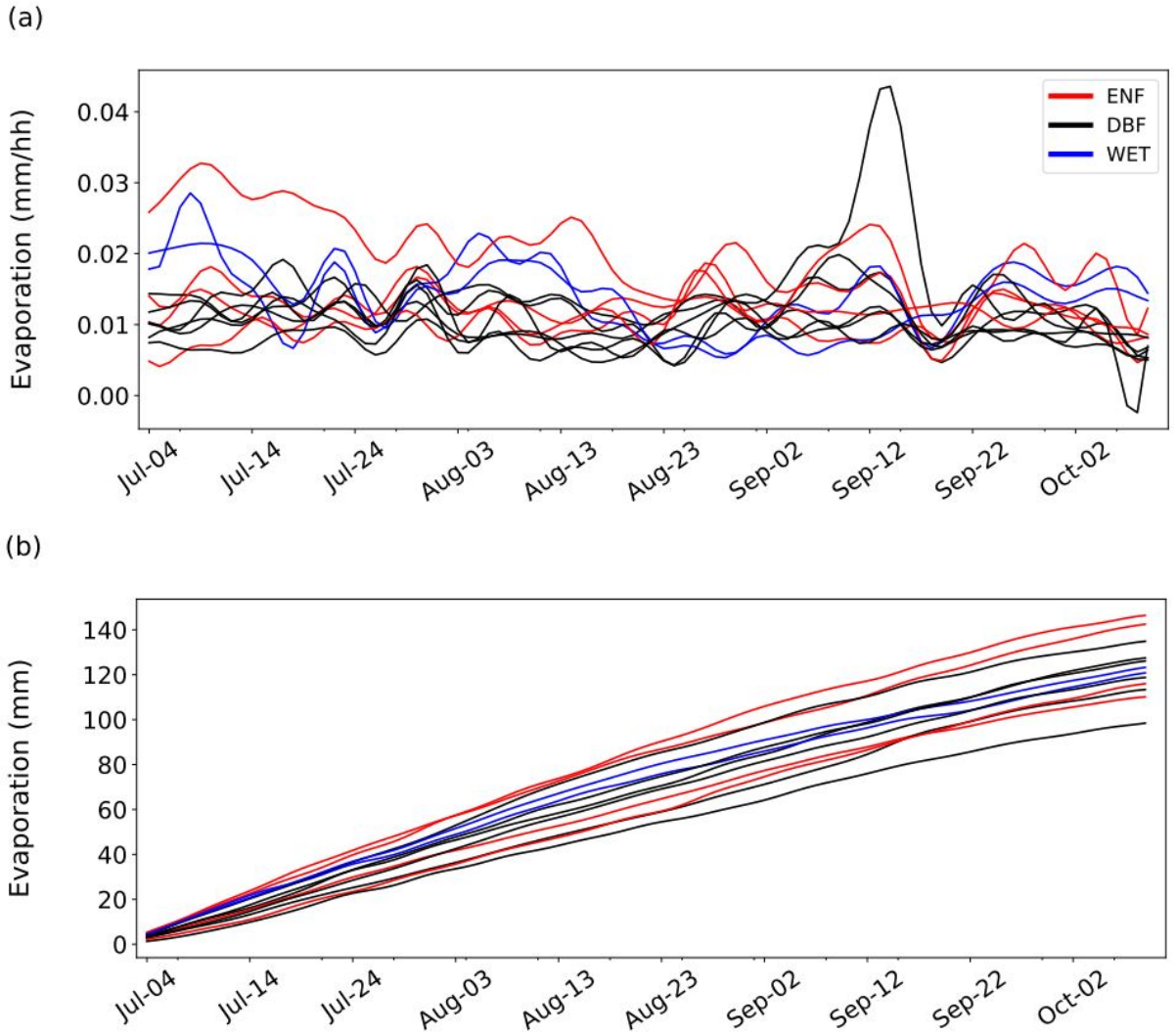

Figure 6. (a) The daily median evaporation (E) from July 3rd to October 11th, 2019, for all sites smoothed with a Butterworth filter (b) cumulative sum across all sites. ENF sites are denoted in red, deciduous sites in black, and wetlands in blue.

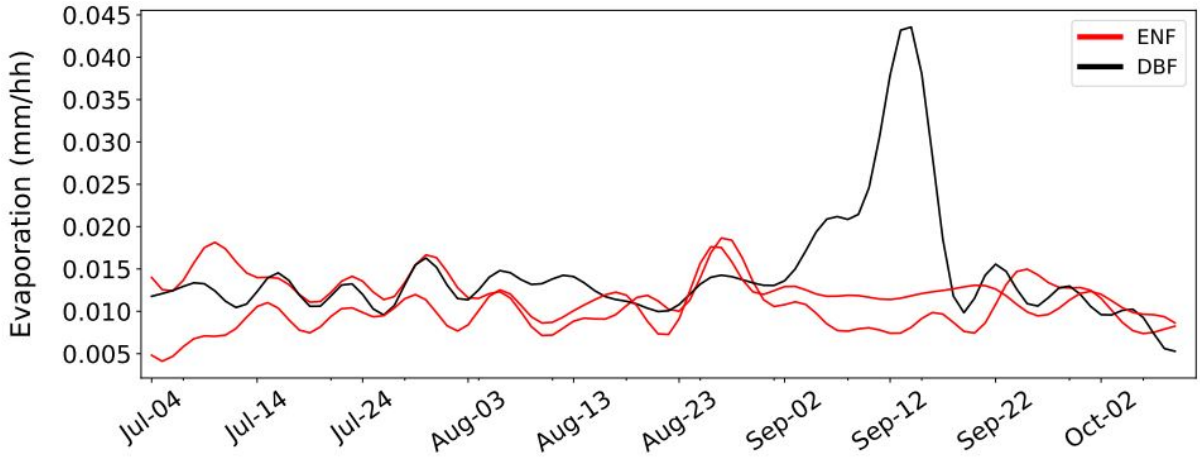

Figure 7. The daily median evaporation from July 3rd to October 11th, 2019, for 3 sites: NE2, SE2, SE6, smoothed with a Butterworth filter to show soil texture differences. A deciduous broadleaf forest with loam (SE2) is denoted in black and two evergreen needle leaf forests on sandy soils are denoted in red for comparison.

FVS-partitioned E across all sites was more aseasonal than perhaps expected (Figure 6a) and the seasonal sum of E for tussock flow-through wetlands (123 mm) was not significantly different from the mean of the forested sites (124 mm) (Figure 6b). Mean LEe was significantly different among most sites, using pairwise comparison, but LEe at SW1 and NE2 was not significantly different to most other sites due to their larger standard errors (Table S3). The site with highest E (147 mm), NE2, was dominated by pine and fir spruce, while the site with the lowest E was SW4 (100 mm), a mixed hardwood forest. A few sites had generally higher evaporation during the summer, notably NW4 (Figure 5a), but most followed a relatively constant daily trend until September 12 when there was an increase in E across all sites. This followed a significant rain event the day before, as well as two large rain events on 3rd and 5th of September. Soil water content also peaked on this day (Figure S1).

Soil data was used from the NRCS Soil Survey to categorize the dominant soil type for most of the flux footprint at each site in order to capture soil texture on an ecosystem scale. Of the 17 sites, 5 were sandy soils, one was a loam, and the rest were sandy loams (Table 1). The site with the loam soil exhibited a large increase in E on September 14th after the large storm event on September 3rd, followed by smaller rain events on September 5th, and 11-13th (Figure 7), when soil water content also peaked (Figure 4b and S1).

3.5 Transpiration

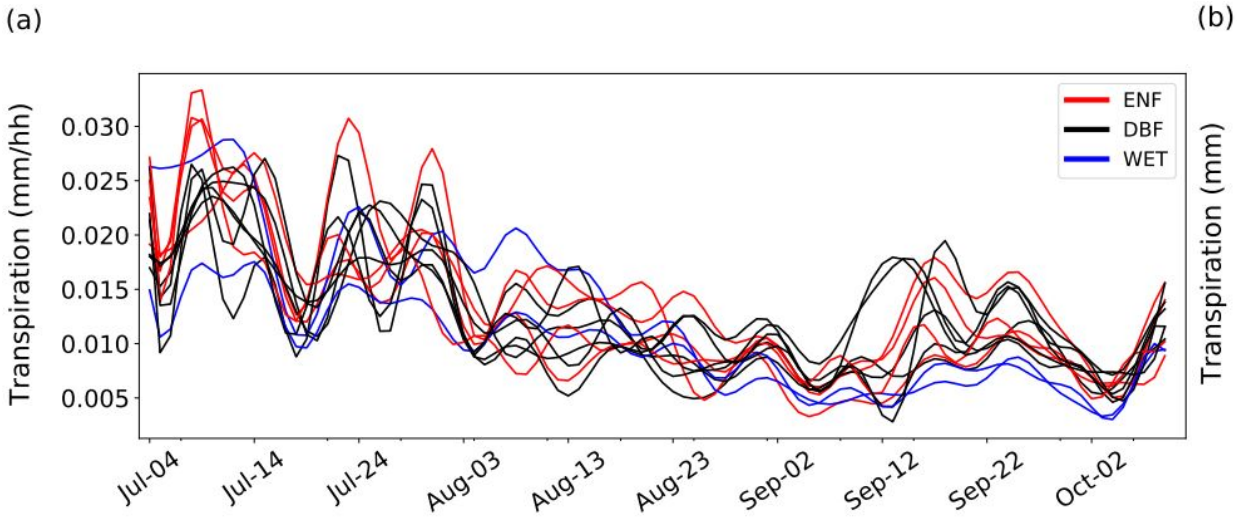

Figure 8. (a) The daily median transpiration from July 3rd to October 11th, 2019, for all sites smoothed with a Butterworth filter (b) cumulative sum across all sites. ENF sites are denoted in red, DBF sites in black, and wetlands in blue.

T decreased steadily, on average, throughout the study period along with the decline in Rn (Figure 3a) which explained about 68% of its variance, on average, across all sites. This is evident in the cumulative sum which begins to flatten out starting late-August, following a significant drop in Rn in early September (Figure 3a and 8b) during and after the precipitation events (Figure 4a). Mean LEt was significantly different across most ecosystems (Table S4). SW3, a dense mixed DBF, had the highest cumulative T (197 mm), while NW1, a pine and spruce/fir forest, had the lowest amongst forest sites (163 mm). Wetland sites transpired significantly less than the forested sites on average (121 mm) across the measurement period, while forest T averaged 178 mm ($P<0.0001$). There was a period of increased transpiration in mid-September, following the large precipitation events (Figure 4A).

3.6 The E/ET and T/ET ratios

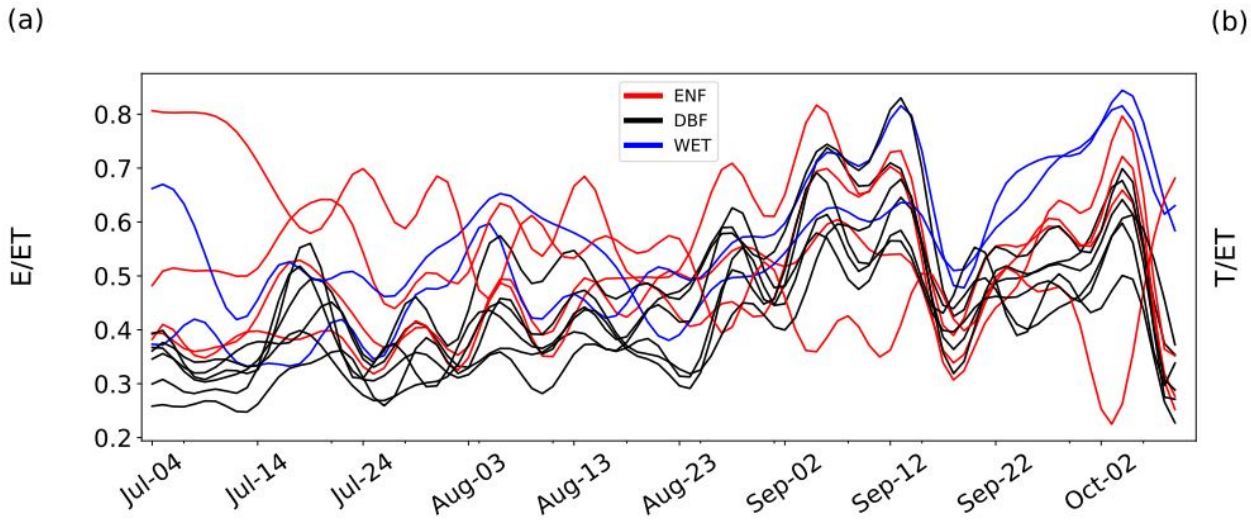

Figure 9. The daily median of (a) E/ET and (b) T/ET for all sites from July 3rd to October 11th, 2019, smoothed using a Butterworth filter for visualization. ENF sites are denoted in red, DBF sites in black, and wetlands in blue. 3.

E/ET (Figure 9a) increased, and T/ET (Figure 9b) decreased, on average, over the course of the study with a notable increase in E/ET (and corresponding decrease in T/ET) in early September during the wet period. Because ET decreased (Figure 5a) and E remained relatively constant across the study period (Figure 6a), E/ET increased during that time (Figure 9a). Average T/ET for all sites over the course of the entire study was 52% and averaged 46.0% at the wetland sites, 52.6% at the ENF sites, and 54.3% at the DBF sites.

3.7 Uncertainty analysis

The range of uncertainties in the FVS-partitioned water fluxes, calculated as the combination of random measurement uncertainty and gap filling uncertainty, ranged from 3.0% to 6.3% for LE (Table S5), 4.1% to 7.8% for LEt (Table S6) and 5.3% to 10.5% for LEe (Table S7).

4 Discussion

4.1 Overview

Partitioning ET to increase our understanding of the hydrologic components is becoming increasingly important for water resource management in a changing climate. While transpiration and evaporation fluxes can be readily measured at point or individual tree scales, it remains difficult to measure at ecosystem scale across multiple sites. This study attempts to address this using a dense array of 17 eddy covariance towers in a 10×10 km^2 area of which 12 ecosystems had a higher proportion of Fluxpart algorithm convergence. We hypothesized that wetlands and the forests will partition E and T differently during the

seasonal transition from early July to early October in northern Wisconsin and expected T to dominate ET in the summer and decrease into autumn with little differentiation between ecosystem types, while E should dominate in forested ecosystems in autumn due to loss of transpirable surfaces and that T will differ little amongst forest ecosystems following relative insensitivity to forest type (Oishi et al., 2010; Roberts, 1983).

We found that ET decreased (Figure 5a) when energy inputs into the characteristically energy-limited ecosystems decreased (Figure 3a) as expected. This seasonal decline in ET was dominated by a corresponding decline in T (Figure 8a), whereas E was largely aseasonal across the measurement period (Figure 6a) with little difference among ecosystems in its cumulative sum despite different responses to wet conditions due to soil texture (Figure 6b). The cumulative sum of T across the measurement period differed little among forests as anticipated, despite differences in forest composition. We describe the FVS partitioning outcomes that resulted in these findings before describing seasonal patterns of fluxes and their responses to micrometeorological variability across different ecosystems.

4.2 FVS Partitioning

Towers were placed in a quasi-random nature to address the CHEESEHEAD19 study objectives to understand the role of landscape heterogeneity in mesoscale atmospheric dynamics (Butterworth et al., 2021). As a result, some towers were located in less-than-ideal flux measurement terrain including near vegetation transitions and at the aquatic/terrestrial interface, which contributed to the lack of Fluxpart algorithm success in some cases. Partitioning results were not obtained at NE1 because the Fluxpart models for estimating water use efficiency require the instrument height to be above the canopy height (Table 1). The Fluxpart algorithm often failed at the wetland sites due to "negative VPD", which is consistent with the challenges of precisely calibrating humidity measurements near saturation (Meyer et al., 2008) noting that the near-surface air at the wetland ecosystems had lower VPD on average (Figure 4d).

Partitioning success is influenced by scalar-scalar correlations such as water vapor (q) and carbon dioxide (c) concentrations, which in turn are influenced by sink-source distribution, height (atmospheric surface layer, roughness sublayer), surface heterogeneity, and canopy density (Skaggs et al., 2018; Klosterhalfen et al., 2019). As mentioned previously, towers were not always placed in optimal positions and in addition to the inherent heterogeneity of the ecosystem surface, senescence of deciduous foliage produced additional patchiness to the landscape which can be an important factor in validity of scalar similarity, and may have interfered with scalar-scalar relations (Williams et al., 2007). We examined the relationship between partitioning success and site characteristics and found no significant correlation between LAI, the canopy height or instrument height. There was a weak positive correlation ($R^2 = 0.30$) between the distance between the canopy and instrument height and partitioning success. A previous study (Klosterhalfen et al. 2019) found that partitioning success was

correlated positively to the instrument to canopy height ratio, overall canopy height, instrument height, and LAI. However, this was concluded using large eddy simulation outputs and may therefore differ from field observations of heterogeneous ecosystems. We found no correlation between partitioning success and the canopy to instrument height ratio, and no correlation to canopy or instrument height individually. If sampling heights are too far from the canopy, turbulence would likely fully mix the air parcel and distinguishing the scalars via partitioning may therefore no longer be accurate (Klosterhalfen et al. 2019, Zahn et al., 2022). For which Zahn et al. (2022) recommends an instrument to canopy height ratio (z/h) of less than or equal to 2, to fall outside of the roughness sublayer but not be too far above the canopy for flux partitioning algorithms like FVS. Of our 17 sites, 7 fell outside of this range, one of which being within the roughness sublayer. Zahn et al. (2022) also found when compared to two other partitioning methods, FVS had the lowest rate of convergence because of frequent failure to satisfy its assumptions, principally because of missing observational data. The main source of uncertainty arises from approximations used to represent the correlation coefficient between carbon and water vapor components. Despite the limitations of any flux partitioning approach, FVS provided novel insights into E and T in this study that help us understand the ecohydrology of multiple different ecosystems within a landscape.

4.3 Controls over Evaporation

E was largely aseasonal across the study period and remained the daily sum of E varied little throughout the shift from late June until mid-October (Figure 6b). This finding is supported by Paul-Limoges (2020) who also found quasi-constant daily E below the canopy throughout seasonal changes in a deciduous forest in Switzerland. E is strongly associated with changes in soil moisture under water limited conditions (Or & Lehmann, 2019; Perez-Priego et al., 2018); however as long as the moisture content of the soil surface is close to saturation, atmospheric conditions control E, which begs the question of why it varied little during our measurement campaign as Rn decreased.

An explanation follows from recent advances in soil E modeling. Based on the widely used equation proposed by Gardner (1959) which suggests that evaporation decreases as a function of the square root of time following precipitation events, Brutsaert (2014) proposed an exponential decay function of soil moisture drawdown. Or & Lehmann (2019) introduced a model based on the notion that soil is an 'evaporative capacitor' with recharge and discharge based on precipitation statistics and soil physical characteristics. In this model, stage-I of drying soil is governed by atmospheric conditions, as capillary flow through the soil is sufficient to satisfy evaporative demand and E is only limited by available energy in the gradient between upper layers of the soil and the atmosphere. During stage-II, E becomes primarily a function of soil water content and soil hydraulic properties: evaporation rates drop significantly as the soil continues to dry and the system becomes water-limited. The transition between the first and second stage is dictated by storage, the product of average water content

and the characteristic length (L_c) of the soil – the limiting depth for capillary extraction of water from deeper soils – which varies by soil texture, with shorter lengths for both coarse and fine-textured soils (Or & Lehmann 2019). The characteristic length is considered a good indicator to encompass soil hydraulic properties' effect on evaporation (Schneider et al., 2021).

We can examine our observations in the context of these models. Frequent precipitation inputs in our study domain are consistent with a situation where the time-varying component of E during dry-downs played a minor role in the observed time-series, on average. The range in soil textures across the study domain indicated that we would expect to see evaporative differences at some sites during stage-II drying, i.e. sandy soils should evaporate less than other sites. We found evidence of this with a large increase in E after the early September rain events at the loam site (Figure 7), consistent with a lower infiltration rate in loam soils. We found that while mean E at most sites was statistically different from each other, there was very little overall difference in cumulative LEe between them despite the variability in soil type. This is consistent with the notion that the ecosystems were never water-limited in a way that would influence evaporation rates due to L_c. Soil moisture was variable throughout the summer but tended to increase through the fall (Table S1), keeping characteristic lengths short and E largely under atmospheric control. This is supported by Schneider et al. (2021) who found no difference in E between different soil types, while other studies have found distinct differences between evaporation and soil texture at water-limited sites (Merlin et al., 2016).

During autumn, as total Rn decreases (Figure 3a) more sunlight can penetrate the canopy as leaves begin to fall during senescence, especially in the DBF forests. We posit that declining leaf area compensated for declining Rn through the seasonal transition such that changes in subcanopy Rn were muted, such that the subcanopy Rn declined at a lower rate than above-canopy Rn. Coupled with sporadic precipitation events which maintained soil moisture levels in the later months, E/ET increased (Figure 9a) as T declined (Figure 8a). This resulted in a situation where E is quasi-constant throughout the season while T declined steadily due to its close coupling with Rn.

4.4 Controls over transpiration

T is driven by differences in atmospheric water and soil water potentials but unlike E, is regulated through plant stomata. Rn dictated T, which explained 68% of the average variance across all sites in our energy-limited ecosystems. Water availability was not limiting, and canopy conductance was unaffected during the pluvial study year. High VPD typically causes plants to close their stomata to minimize water loss (Monteith 1995), but high VPD conditions tend to co-occur with high radiation therefore making it difficult to separate their effects (Grossiord et al. 2020). Transpiration rates increase as VPD increases to a certain threshold depending on the ecosystem (Ficklin & Novick, 2017; Franks et al., 1997; Marchin et al., 2016; Sulman et al., 2016; Will et al., 2013). This consumptive behavior is a reflection of environments that are not water-

limited, such that gas exchange is maximized (Sadok et al., 2021). Accordingly, stomata respond to changes in radiation such that T changes in proportion to the radiation load (Pieruschka et al., 2010). The ecosystems studied here were controlled by Rn and consequentially T, and while T increased VPD, it rarely reached the limiting threshold of 1 kPa (Körner, 1995; Oren et al., 1999), as VPD remained below this threshold 90% of the time.

4.5 T/ET

Average T/ET from the July to October study period was 52.3% across all sites, with an average of 54.5% among the forested sites and 46.0% among the wetland sites. These numbers fall within the wide range established by many previous global studies of various ecosystems of 40 to 90% (Good et al., 2015; Schlesinger & Jasechko, 2014; L. Wang et al., 2014; Wei et al., 2017a; Zhou et al., 2016). This study is on the lower end of the previously reported range of 40 to 86% for temperate forests (Schlesinger & Jasechko, 2014) and is lower than estimates generated using isotopic approaches on the order of 64% (Good et al., 2015). However, Paschalis et al. (2018) found a significant decline in T/ET when moving from dry to wetter areas – about a 10% change – which may explain why we see lower T/ET than some other studies in our energy-limited, but not water limited ecosystems, as precipitation during 2019 exceeded annual averages compared to previous years.

Wang et al. (2014) showed an exponential relationship between LAI and T/ET indicating that vegetative control over T/ET occurs over the lower LAI range. However, when only natural vegetation sites (with LAI>1) were considered, there was a negligible dependence of T/ET on LAI (Paschalis et al. 2018). LAI data collected for 5 mixed forest sites on June 25th (NE2, NE4, SE3, SE6, SW4) revealed no relationship between T/ET and LAI, however, all sites had LAI>1. This finding is supported by Fatichi and Pappas (2017) and Berkelhammer et al. (2016) who found that LAI matched seasonal dynamics of T/ET but not diel, daily or annual timescales. In contrast, Nelson et al. (2020) found that T/ET varied much more between sites than different years at the same site, indicating more reliance on site characteristics than climatic variables.

Wetland T/ET is significantly altered by structural factors such as open water, plant species and diversity, as well as environmental factors like diurnal fluctuations in air and water temperature and water table depths (Drexler et al., 2004; Eichelmann et al., 2018). Between wetland sites the most important factor affecting ET levels is the proportion of open water versus vegetation cover (Eichelmann et al. 2018). Shorter vegetation, such as tussock grasses which can often be found in wetlands, optimize leaf structure to minimize water loss in light rich environments (Givnish, 1988) resulting in lower transpiration but greater WUE compared to forested sites. As the area of open water increases, E increases more than T, as we found evidence of decreased T/ET in wetlands compared to the forested sites.

4.6 Uncertainty analysis

Uncertainties in the FVS-partitioned water fluxes ranged between 3.0% and 10.5%, which was similar to or slightly larger than random measurement uncertainties (3-6%) from other forested ecosystems (Goulden et al., 1996; Oren et al., 2006; Stoy et al., 2006). Earlier approaches assumed that LE can be gap filled with a high degree of success due to their relatively predictable response to environmental conditions (Falge et al., 2001). For example, REddyProc tends to estimate gaps in latent heat flux measurements with a low degree of uncertainty (Foltýnová et al., 2020). Nevertheless, future efforts should examine the ability of gap filling methods to accurately simulate LEt and LEe. More complex LE gap filling methods are being developed (e.g. Khan et al., 2021) but it needs to be determined if they will offer improved predictive skill. We elected not to estimate the "spatial" uncertainty of estimating heterogeneous ecosystems using a single point measurement (Oren et al., 2006) as we did not have multiple towers in individual ecosystems to do so and sought to avoid unconstrained estimation. We also had little basis for estimating bias errors including potential underestimation of LE due to the known challenges of lack of energy balance closure of eddy covariance measurements (Foken, 2008; Leuning et al., 2012; Stoy et al., 2013). However, independent approaches are converging on the notion that underestimated turbulent flux terms may be due more to sensible than latent heat fluxes (Charuchittipan et al., 2014; Gerken et al., 2018; Mauder et al., 2020), suggesting low variability, more or less independent of the energy balance closure. Ongoing efforts to parameterize underestimated turbulent fluxes require estimates of atmospheric boundary layer heights (Mauder et al., 2021), which are difficult to quantify using individual flux towers (Beamesderfer et al., in review), but the extensive land surface and atmospheric observations available from CHEESEHEAD19 (Butterworth et al., 2021) provide opportunities to better-understand potential bias uncertainties in eddy covariance measurements.

It is important to note that unknown uncertainties discussed above and different methods to estimate WUE in the FVS algorithm also impact results. FVS may overestimate soil E (Klosterhalfen et al., 2019) while conditional sampling methods (Thomas et al., 2008; Zahn et al., 2022) may underestimate it in comparison to respiration chamber measurements, with implications for our understanding of E and T. For reference on comparisons of FVS to leaf-level measurements see Scanlon et al., 2019, and for comparison to other partitioning methods see Nelson et al., 2020 and Klosterhalfen et al., 2019. Ongoing efforts to improve water flux partitioning including optimality solutions for WUE in flux variance similarity (Scanlon et al., 2019) and new conditional sampling methodologies (Zahn et al., 2022) will ideally improve the accuracy of these methods to create defensible estimates of water flux terms.

4.7 Implications for forests, wetlands, and water management

Our results have implications for forest hydrology but few studies have looked at the influence of forest management practices on evapotranspiration (Komatsu & Kume, 2020). Practices like forest thinning are commonly used as a water

saving strategy but are understudied, particularly in wet environments (Sun et al., 2017). Forest thinning, which influences ET partitioning with increased light penetration due to a more open canopy, alters the microclimate of the ground layer. Sun et al. (2017) found that ET decreased by 20% after thinning, yielding an increase in water yield to the watershed, as supported by other studies (Dung et al., 2012; Hawthorne et al., 2013). Most forest hydrology research involves changes in runoff rather than change in ET; this omission – due in part to the relative difficulties in measuring ET versus runoff – can hinder accurate modeling and therefore optimal management (Komatsu and Kume 2020).

Wetlands are essential climate regulators, but unfortunately are globally declining three times faster than forests, with most losses due to land use change, agriculture and climate change (Finlayson & Davidson, 2018; Granata et al., 2020). Considering both wetland losses and wetland restoration efforts underway, such as converting crop lands back to wetlands (WDNR 2008), understanding the hydrologic changes is imperative. Difference in evapotranspiration from wetland sites (especially with open water) is significant compared to drained agricultural sites, with much higher ET in the wetlands (Eichelmann et al. 2018). Not only is ET higher, but the use of water is much different; T/ET has found to be between 31-37% in wetlands but on the order of 70% in the cropping systems that often replace them (Wang-Erlandsson et al., 2014; Wei et al., 2017b). Additionally, increasing global temperatures could have significant implications for evaporative loss from wetlands as it has been shown that air and water temperatures are strong drivers of nighttime ET, which is dominated by E in these systems (Eichelmann et al. 2018; 2022). When wetlands are drained there are detrimental effects for water storage and groundwater inflation (van der Kamp & Hayashi, 2009); improving our understanding of the contributions of E and T to ET is essential to understanding land use and climate change impacts on water cycling in these systems.

4.8 Future work

Remote sensing has become a promising and dominant approach to be able to quantify global ET (Mu et al., 2007; K. Zhang et al., 2016). Currently algorithms are able to model E and T separately, however, these have never been independently validated across multiple ecosystems using observations (Talsma et al., 2018). A key advantage of eddy covariance is the continuous, sub-daily sampling and spatial scale of the measurements which can easily be linked to remote sensing products (Chu et al., 2017). Among ET detecting sensors are Landsat, MODIS, Sentinel GOES and ECOSTRESS, a thermal radiometer on the International space station which produces thermally derived ET at 70 m resolution (Fisher et al., 2017), aligning with characteristic length scales of eddy covariance flux footprints. This allows for validation of the new ECOSTRESS algorithm which uses the PT-JPL model to estimate E and T from the land surface (Fisher et al., 2008, 2017). Remote sensing can aid in coverage of larger areas and address some of the representativeness problems of our current technology and instrumentation (Schimel et al., 2015), and can be used

to understand local hydrologic cycling more comprehensively. However, land surface heterogeneity is an inevitable problem in calculating ET with coarse resolution (Burchard-Levine et al., 2021) and land surface heterogeneity can cause errors in LE (Butterworth et al., 2021; Liu et al., 2016). Therefore, addressing the problem of land surface heterogeneity is crucial for a more accurate ET estimation.

5 Conclusion

This study applies the flux variance similarity method to partition ET using high frequency data from eddy covariance towers to investigate the role of vegetation and seasonal dynamics in E and T. On average T accounted for 54.5% of ET at forested sites and 46.0% for wetlands, emphasizing a lower contribution of E in forests. E was relatively aseasonal and independent of ecosystem type throughout the study period due to the frequent precipitation but differed after large precipitation events as a function of soil type, where loam soils tended to have greater E following compounding rain events. T is highly correlated with climatic variables depending on the ecosystem, which varied between wetlands and forested ecosystems. While minimal, DBF ecosystems tended to have greater T compared to coniferous forests. Wisconsin has seen a 15% increase in annual precipitation since 1950, with most extreme increases dominated by seasonal transitions, spring and fall, and this trend is expected to maintain (WICCI 2020). Therefore partitioning ET into its components during a seasonal transition in a wet year across various ecosystems provides new insights for understanding how different ecosystems use water with implications for hydrologic modeling in an era of rapid land use and climate change.

Acknowledgments

CHEESEHEAD19 was primarily supported from the National Science Foundation award #1822420 in addition to support from the DOE Ameriflux Network Management Project and NOAA. Brian Butterworth was additionally supported by the NOAA Physical Sciences Laboratory. NOAASURFRAD measurements were provided by NOAA's Climate Program Office, Climate Observations and Monitoring Program project number NA20OAR4310338. We thank NCAR's Earth Observing Laboratory, sponsored by the National Science Foundation for their operational, technical, and scientific support. We thank Anita Thompson for insightful comments on the manuscript. This project would not be possible without the support provided by the U.S. Forest Service and Wisconsin Educational Communications Board. We wish to acknowledge the Indigenous Nations on whose ancestral lands and ceded territories the study took place and recognize that the infrastructure used for this project is built on Indigenous land. We recognize the Ojibwe people as past, present, and future caretakers of this land whose stewardship of the region was interrupted through their physical removal by the 1830 Indian Removal Act and through US Assimilation policies explicitly designed to eradicate Indigenous language and ways of being until the 1970s. We are aware of no conflicts of interest

Open Research

All eddy covariance data are published by Ameriflux at https://ameriflux.lbl.gov or have been submitted for data publication. CHEESEHEAD19 observations including surface radiation and high-frequency flux time series are archived by UCAR at https://www.eol.ucar.edu/field_projects/cheesehead. FVS-partitioned flux data are published on Figshare at https://doi.org/10.6084/m9.figshare.20110796.v1. Soils data are available online at: http://websoilsurvey.sc.egov.usda.gov/ by the Soil Survey Staff, Natural Resources Conservation Service, United States Department of Agriculture.

References

Anderson, R. G., Zhang, X., & Skaggs, T. H. (2017). Measurement and Partitioning of Evapotranspiration for Application to Vadose Zone Studies. *Vadose Zone Journal*, *16*(13), 1–9. https://doi.org/10.2136/VZJ2017.08.0155Baldocchi, D. (2014). Measuring fluxes of trace gases and energy between ecosystems and the atmosphere – the state and future of the eddy covariance method. *Global Change Biology*, *20*(12), 3600–3609. https://doi.org/10.1111/GCB.12649Beck, H. E., Zimmermann, N. E., McVicar, T. R., Vergopolan, N., Berg, A., & Wood, E. F. (2018). Present and future Köppen-Geiger climate classification maps at 1-km resolution. *Scientific Data*, *5*(1), 180214. https://doi.org/10.1038/sdata.2018.214Berkelhammer, M., Noone, D. C., Wong, T. E., Burns, S. P., Knowles, J. F., Kaushik, A., Blanken, P. D., & Williams, M. W. (2016). Convergent approaches to determine an ecosystem's transpiration fraction. *Global Biogeochemical Cycles*, *30*(6), 933–951. https://doi.org/10.1002/2016GB005392Brutsaert, W. (2016). Global land surface evaporation trend during the past half century: Corroboration by Clausius-Clapeyron scaling. *Advances in Water Resources*, *106*, 3–5. https://doi.org/10.1016/j.advwatres.2016.08.014Burchard-Levine, V., Nieto, H., Riaño, D., Migliavacca, M., El-Madany, T. S., Guzinski, R., Carrara, A., & Martín, M. P. (2021). *The effect of pixel heterogeneity for remote sensing based retrievals of evapotranspiration in a semi-arid tree-grass ecosystem*. https://pubag.nal.usda.gov/catalog/7347985Butterworth, B. J., Desai, A. R., Metzger, S., Townsend, P. A., Schwartz, M. D., Petty, G. W., Mauder, M., Vogelmann, H., Andresen, C. G., Augustine, T. J., Bertram, T. H., Brown, W. O. J., Buban, M., Cleary, P., Durden, D. J., Florian, C. R., Iglinski, T. J., Kruger, E. L., Lantz, K., … Zheng, T. (2021). Connecting Land–Atmosphere Interactions to Surface Heterogeneity in CHEESEHEAD19. *Bulletin of the American Meteorological Society*, *102*(2), E421–E445. https://doi.org/10.1175/BAMS-D-19-0346.1Campbell, G. S., & Norman, J. M. (1998). An Introduction to Environmental Biophysics. *An Introduction to Environmental Biophysics*. https://doi.org/10.1007/978-1-4612-1626-1Charuchittipan, D., Babel, W., Mauder, M., Leps, J.-P., & Foken, T. (2014). Extension of the Averaging Time in Eddy-Covariance Measurements and Its Effect on the Energy Balance Closure. *Boundary-Layer Meteorology*, *152*(3), 303–327.

https://doi.org/10.1007/s10546-014-9922-6Chu, H., Baldocchi, D. D., John, R., Wolf, S., & Reichstein, M. (2017). Fluxes all of the time? A primer on the temporal representativeness of FLUXNET. *Journal of Geophysical Research: Biogeosciences*, *122*(2), 289–307. https://doi.org/10.1002/2016JG003576Davis, K. J., Yi, C., & Berger, B. W. (2003). *The annual cycles of CO2 and H2O exchange over a northern mixed forest as observed from a very tall tower*. https://doi.org/10.1046/j.1365-2486.2003.00672.xDesai, A. R., Khan, A. M., Zheng, T., Paleri, S., Butterworth, B., Lee, T. R., Fisher, J. B., Hulley, G., Kleynhans, T., Gerace, A., Townsend, P. A., Stoy, P., & Metzger, S. (2021). Multi-Sensor Approach for High Space and Time Resolution Land Surface Temperature. *Earth and Space Science*, *8*(10), e2021EA001842-e2021EA001842. https://doi.org/10.1029/2021EA001842Detto, M., & Katul, G. G. (2007). Simplified expressions for adjusting higher-order turbulent statistics obtained from open path gas analyzers. *Boundary-Layer Meteorology*, *122*(1), 205–216. https://doi.org/10.1007/s10546-006-9105-1Drexler, J. Z., Snyder, R. L., Spano, D., & Paw U, K. T. (2004). A review of models and micrometeorological methods used to estimate wetland evapotranspiration. *Hydrological Processes*, *18*(11), 2071–2101. https://doi.org/10.1002/hyp.1462Dung, B. X., Gomi, T., Miyata, S., Sidle, R. C., Kosugi, K., & Onda, Y. (2012). Runoff responses to forest thinning at plot and catchment scales in a headwater catchment draining Japanese cypress forest. *Journal of Hydrology*, *444–445*, 51–62. https://doi.org/10.1016/j.jhydrol.2012.03.040Eichelmann, E., Hemes, K. S., Knox, S. H., Oikawa, P. Y., Chamberlain, S. D., Sturtevant, C., Verfaillie, J., & Baldocchi, D. D. (2018). The effect of land cover type and structure on evapotranspiration from agricultural and wetland sites in the Sacramento–San Joaquin River Delta, California. *Agricultural and Forest Meteorology*, *256–257*, 179–195. https://doi.org/10.1016/j.agrformet.2018.03.007Eicker, A., Forootan, E., Springer, A., Longuevergne, L., & Kusche, J. (2016). Does GRACE see the terrestrial water cycle "intensifying"? *Journal of Geophysical Research: Atmospheres*, *121*(2), 733–745. https://doi.org/10.1002/2015JD023808Falge, E., Baldocchi, D., Olson, R., Anthoni, P., Aubinet, M., Bernhofer, C., Burba, G., Ceulemans, R., Clement, R., Dolman, H., Granier, A., Gross, P., Grünwald, T., Hollinger, D., Jensen, N.-O., Katul, G., Keronen, P., Kowalski, A., Ta Lai, C., … Wofsy, S. (2001). Gap filling strategies for long term energy flux data sets. *Agricultural and Forest Meteorology*, *107*(1), 71–77. https://doi.org/10.1016/S0168-1923(00)00235-5Fatichi, S., & Pappas, C. (2017). Constrained variability of modeled T:ET ratio across biomes. *Geophysical Research Letters*, *44*(13), 6795–6803. https://doi.org/10.1002/2017GL074041Ficklin, D. L., & Novick, K. A. (2017). Historic and projected changes in vapor pressure deficit suggest a continental-scale drying of the United States atmosphere. *Journal of Geophysical Research: Atmospheres*, *122*(4), 2061–2079. https://doi.org/10.1002/2016JD025855Finlayson, M., & Davidson, N. (2018). *Global wetland outlook: Technical note on status and trends*. Secretariat of the Ramsar Convention.Fisher, J. B., Melton, F., Middleton, E., Hain, C., Anderson, M., Allen, R., Mccabe, M. F., Hook, S., Baldocchi, D., Townsend, P. A., Kilic, A., Tu, K., Miralles, D. D., Perret, J., Lagouarde,

J.-P., Waliser, D., Purdy, A. J., French, A., Schimel, D., … Wood, E. F. (2017). *The future of evapotranspiration: Global requirements for ecosystem functioning, carbon and climate feedbacks, agricultural management, and water resources*. https://doi.org/10.1002/2016WR020175Fisher, J. B., Tu, K. P., & Baldocchi, D. D. (2008). Global estimates of the land–atmosphere water flux based on monthly AVHRR and ISLSCP-II data, validated at 16 FLUXNET sites. *Remote Sensing of Environment*, *112*(3), 901–919. https://doi.org/10.1016/j.rse.2007.06.025Foken, T. (2008). The Energy Balance Closure Problem: An Overview. *Ecological Applications*, *18*(6), 1351–1367. https://doi.org/10.1890/06-0922.1Foltýnová, L., Fischer, M., & McGloin, R. P. (2020). Recommendations for gap-filling eddy covariance latent heat flux measurements using marginal distribution sampling. *Theoretical and Applied Climatology*, *139*(1), 677–688. https://doi.org/10.1007/s00704-019-02975-wFranks, P. J., Cowan, I. R., & Farquhar, G. D. (1997). The apparent feedforward response of stomata to air vapour pressure deficit: Information revealed by different experimental procedures with two rainforest trees. *Plant, Cell & Environment*, *20*(1), 142–145. https://doi.org/10.1046/j.1365-3040.1997.d01-14.xGardner, W. R. (1959). *Solutions of the Flow Equation for the Drying of Soils and Other Porous Media 1*. https://doi.org/10.2136/sssaj1959.03615995002300030010xGerken, T., Ruddell, B. L., Fuentes, J. D., Araújo, A., Brunsell, N. A., Maia, J., Manzi, A., Mercer, J., dos Santos, R. N., von Randow, C., & Stoy, P. C. (2018). Investigating the mechanisms responsible for the lack of surface energy balance closure in a central Amazonian tropical rainforest. *Agricultural and Forest Meteorology*, *255*, 92–103. https://doi.org/10.1016/j.agrformet.2017.03.023Givnish, T. (1988). Adaptation to Sun and Shade: A Whole-Plant Perspective. *Functional Plant Biology*, *15*(2), 63. https://doi.org/10.1071/PP9880063Good, S. P., Noone, D., & Bowen, G. (2015). Hydrologic connectivity constrains partitioning of global terrestrial water fluxes. *Science*, *349*(6244), 175–177. https://doi.org/10.1126/SCIENCE.AAA5931/SUPPL_FILE/AAA5931-GOOD-SM.PDFGoulden, M. L., Munger, J. W., Fan, S.-M., Daube, B. C., & Wofsy, S. C. (1996). Measurements of carbon sequestration by long-term eddy covariance: Methods and a critical evaluation of accuracy. *Global Change Biology*, *2*(3), 169–182. https://doi.org/10.1111/j.1365-2486.1996.tb00070.xGranata, F., Gargano, R., & de Marinis, G. (2020). Artificial intelligence based approaches to evaluate actual evapotranspiration in wetlands. *Science of The Total Environment*, *703*, 135653. https://doi.org/10.1016/j.scitotenv.2019.135653Hawthorne, S. N. D., Lane, P. N. J., Bren, L. J., & Sims, N. C. (2013). The long term effects of thinning treatments on vegetation structure and water yield. *Forest Ecology and Management*, *310*, 983–993. https://doi.org/10.1016/j.foreco.2013.09.046Henderson-Sellers, B. (1984). A new formula for latent heat of vaporization of water as a function of temperature. *Quarterly Journal of the Royal Meteorological Society*, *110*(466), 1186–1190. https://doi.org/10.1002/qj.49711046626Hollinger, D. Y., & Richardson, A. D. (2005). Uncertainty in eddy covariance measurements and its application to physiological models. *Tree Physiology*, *25*(7), 873–885. https://doi.org/10.1093/treephys/25.7.873Huntington, T. G. (2006). Evidence

for intensification of the global water cycle: Review and synthesis. *Journal of Hydrology*, *319*(1–4), 83–95. https://doi.org/10.1016/J.JHYDROL.2005.07.003Jung, M., Reichstein, M., Ciais, P., Seneviratne, S. I., Sheffield, J., Goulden, M. L., Bonan, G., Cescatti, A., Chen, J., de Jeu, R., Johannes Dolman, A., Eugster, W., Gerten, D., Gianelle, D., Gobron, N., Heinke, J., Kimball, J., Law, B. E., Montagnani, L., … Zhang, K. (2010). Recent decline in the global land evapotranspiration trend due to limited moisture supply. *Nature*. https://doi.org/10.1038/nature09396Khan, M. S., Jeon, S. B., & Jeong, M.-H. (2021). Gap-Filling Eddy Covariance Latent Heat Flux: Inter-Comparison of Four Machine Learning Model Predictions and Uncertainties in Forest Ecosystem. *Remote Sensing*, *13*(24), 4976. https://doi.org/10.3390/rs13244976Klosterhalfen, A., Moene, A. F., Schmidt, M., Scanlon, T. M., Vereecken, H., & Graf, A. (2019). Sensitivity analysis of a source partitioning method for H2O and CO2 fluxes based on high frequency eddy covariance data: Findings from field data and large eddy simulations. *Agricultural and Forest Meteorology*, *265*, 152–170. https://doi.org/10.1016/J.AGRFORMET.2018.11.003Komatsu, H., & Kume, T. (2020). Modeling of evapotranspiration changes with forest management practices: A genealogical review. *Journal of Hydrology*, *585*, 124835. https://doi.org/10.1016/j.jhydrol.2020.124835Kool, D., Agam, N., Lazarovitch, N., Heitman, J. L., Sauer, T. J., & Ben-Gal, A. (2014). A review of approaches for evapotranspiration partitioning. *Agricultural and Forest Meteorology*, *184*, 56–70. https://doi.org/10.1016/J.AGRFORMET.2013.09.003Körner, Ch. (1995). Leaf Diffusive Conductances in the Major Vegetation Types of the Globe. In E.-D. Schulze & M. M. Caldwell (Eds.), *Ecophysiology of Photosynthesis* (pp. 463–490). Springer. https://doi.org/10.1007/978-3-642-79354-7_22Kustas, W. P., Anderson, M. C., Alfieri, J. G., Knipppper, K., Torres-Rua, A., Parry, C. K., Nieto, H., Agam, N., White, W. A., Gao, F., McKee, L., Prueger, J. H., Hipppps, L. E., Los, S., Alsina, M. M., Sanchez, L., Sams, B., Dokoozlian, N., McKee, M., … Hain, C. (2018). The Grape Remote Sensing Atmospheric Profile and Evapotranspiration Experiment. *Bulletin of the American Meteorological Society*, *99*(9), 1791–1812. https://doi.org/10.1175/BAMS-D-16-0244.1Leuning, R., van Gorsel, E., Massman, W. J., & Isaac, P. R. (2012). Reflections on the surface energy imbalance problem. *Agricultural and Forest Meteorology*, *156*, 65–74. https://doi.org/10.1016/j.agrformet.2011.12.002Liu, S., Xu, Z., Song, L., Zhao, Q., Ge, Y., Xu, T., Ma, Y., Zhu, Z., Jia, Z., & Zhang, F. (2016). Upscaling evapotranspiration measurements from multi-site to the satellite pixel scale over heterogeneous land surfaces. *Agricultural and Forest Meteorology*, *230–231*, 97–113. https://doi.org/10.1016/j.agrformet.2016.04.008Marchin, R. M., Broadhead, A. A., Bostic, L. E., Dunn, R. R., & Hoffmann, W. A. (2016). Stomatal acclimation to vapour pressure deficit doubles transpiration of small tree seedlings with warming. *Plant, Cell & Environment*, *39*(10), 2221–2234. https://doi.org/10.1111/pce.12790Mauder, M., Foken, T., & Cuxart, J. (2020). Surface-Energy-Balance Closure over Land: A Review. *Boundary-Layer Meteorology*, *177*(2), 395–426. https://doi.org/10.1007/s10546-020-00529-6Mauder,

M., Ibrom, A., Wanner, L., De Roo, F., Brugger, P., Kiese, R., & Pilegaard, K. (2021). Options to correct local turbulent flux measurements for large-scale fluxes using an approach based on large-eddy simulation. *Atmospheric Measurement Techniques*, *14*(12), 7835–7850. https://doi.org/10.5194/amt-14-7835-2021Merlin, O., Stefan, V. G., Amazirh, A., Chanzy, A., Ceschia, E., Er-Raki, S., Gentine, P., Tallec, T., Ezzahar, J., Bircher, S., Beringer, J., & Khabba, S. (2016). Modeling soil evaporation efficiency in a range of soil and atmospheric conditions using a meta-analysis approach. *Water Resources Research*, *52*(5), 3663–3684. https://doi.org/10.1002/2015WR018233Meyer, C. W., Hodges, J. T., Huang, P. H., Miller, W. W., Ripple, D. C., Scace, G. E., Gutierrez, C. M., & Gallagher, P. (2008). *Calibration of Hygrometers with the Hybrid Humidity Generator*. https://doi.org/10.6028/NIST.SP.250-83Mu, Q., Heinsch, F. A., Zhao, M., & Running, S. W. (2007). Development of a global evapotranspiration algorithm based on MODIS and global meteorology data. *Remote Sensing of Environment*, *111*(4), 519–536. https://doi.org/10.1016/j.rse.2007.04.015Nelson, J. A., Pérez-Priego, O., Zhou, S., Poyatos, R., Zhang, Y., Blanken, P. D., Gimeno, T. E., Wohlfahrt, G., Desai, A. R., Gioli, B., Limousin, J. M., Bonal, D., Paul-Limoges, E., Scott, R. L., Varlagin, A., Fuchs, K., Montagnani, L., Wolf, S., Delpierre, N., … Jung, M. (2020). Ecosystem transpiration and evaporation: Insights from three water flux partitioning methods across FLUXNET sites. *Global Change Biology*, *26*(12), 6916–6930. https://doi.org/10.1111/GCB.15314Novick, K. A., Ficklin, D. L., Stoy, P. C., Williams, C. A., Bohrer, G., Oishi, A. C., Papuga, S. A., Blanken, P. D., Noormets, A., Sulman, B. N., Scott, R. L., Wang, L., & Phillips, R. P. (2016). *The increasing importance of atmospheric demand for ecosystem water and carbon fluxes*. https://doi.org/10.1038/NCLIMATE3114Oishi, A. C., Oren, R., Novick, K. A., Palmroth, S., & Katul, G. G. (2010). Interannual Invariability of Forest Evapotranspiration and Its Consequence to Water Flow Downstream. *Ecosystems*, *13*(3), 421–436. https://doi.org/10.1007/s10021-010-9328-3Oki, T., & Kanae, S. (2006). Global Hydrological Cycles and World Water Resources. *New Series*, *313*(5790), 1068–1072.Or, D., & Lehmann, P. (2019). Surface Evaporative Capacitance: How Soil Type and Rainfall Characteristics Affect Global-Scale Surface Evaporation. *Water Resources Research*, *55*(1), 519–539. https://doi.org/10.1029/2018WR024050Oren, R., Hsieh, C.-I., Stoy, P., Albertson, J., Mccarthy, H. R., Harrell, P., & Katul, G. G. (2006). Estimating the uncertainty in annual net ecosystem carbon exchange: Spatial variation in turbulent fluxes and sampling errors in eddy-covariance measurements. *Global Change Biology*, *12*(5), 883–896. https://doi.org/10.1111/j.1365-2486.2006.01131.xOren, R., Sperry, J. S., Katul, G. G., Pataki, D. E., Ewers, B. E., Phillips, N., & Schäfer, K. V. R. (1999). Survey and synthesis of intra- and interspecific variation in stomatal sensitivity to vapour pressure deficit. *Plant, Cell & Environment*, *22*(12), 1515–1526. https://doi.org/10.1046/j.1365-3040.1999.00513.xPalatella, L., Rana, G., & Vitale, D. (2014). Towards a Flux-Partitioning Procedure Based on the Direct Use of High-Frequency Eddy-Covariance Data. *Boundary-Layer Meteorology*, *153*(2), 327–337. https://doi.org/10.1007/S10546-014-9947-X/FIGURES/3Papalexiou, S. M., &

Montanari, A. (n.d.). *Global and Regional Increase of Precipitation Extremes Under Global Warming*. https://doi.org/10.1029/2018WR024067Paul-Limoges, E., Wolf, S., Schneider, F. D., Longo, M., Moorcroft, P., Gharun, M., & Damm, A. (2020). Partitioning evapotranspiration with concurrent eddy covariance measurements in a mixed forest. *Agricultural and Forest Meteorology*, *280*, 107786–107786. https://doi.org/10.1016/J.AGRFORMET.2019.107786Perez-Priego, O., Katul, G., Reichstein, M., El-Madany, T. S., Ahrens, B., Carrara, A., Scanlon, T. M., & Migliavacca, M. (2018). Partitioning Eddy Covariance Water Flux Components Using Physiological and Micrometeorological Approaches. *Journal of Geophysical Research: Biogeosciences*, *123*(10), 3353–3370. https://doi.org/10.1029/2018JG004637Pieruschka, R., Huber, G., & Berry, J. A. (2010). Control of transpiration by radiation. *Proceedings of the National Academy of Sciences*, *107*(30), 13372–13377. https://doi.org/10.1073/pnas.0913177107Prein, A. F., Rasmussen, R. M., Ikeda, K., Liu, C., Clark, M. P., & Holland, G. J. (2017). *The future intensification of hourly precipitation extremes*. https://doi.org/10.1038/NCLIMATE3168Priestley, C. H. B., & Taylor, R. J. (1972). On the Assessment of Surface Heat Flux and Evaporation Using Large-Scale Parameters. *Monthly Weather Review*, *100*(2), 81–92. https://doi.org/10.1175/1520-0493(1972)100<0081:OTAOSH>2.3.CO;2Rana, G., Palatella, L., Scanlon, T. M., Martinelli, N., & Ferrara, R. M. (2018). CO2 and H2O flux partitioning in a Mediterranean cropping system. *Agricultural and Forest Meteorology*, *260–261*, 118–130. https://doi.org/10.1016/J.AGRFORMET.2018.06.007Richardson, A. D., Hollinger, D. Y., Burba, G. G., Davis, K. J., Flanagan, L. B., Katul, G. G., William Munger, J., Ricciuto, D. M., Stoy, P. C., Suyker, A. E., Verma, S. B., & Wofsy, S. C. (2006). A multi-site analysis of random error in tower-based measurements of carbon and energy fluxes. *Agricultural and Forest Meteorology*, *136*(1), 1–18. https://doi.org/10.1016/j.agrformet.2006.01.007Rigden, A. J., Salvucci, G. D., Entekhabi, D., & Short Gianotti, D. J. (2018). Partitioning Evapotranspiration Over the Continental United States Using Weather Station Data. *Geophysical Research Letters*, *45*(18), 9605–9613. https://doi.org/10.1029/2018GL079121Roberts, J. (1983). Forest transpiration: A conservative hydrological process? *Journal of Hydrology*, *66*(1), 133–141. https://doi.org/10.1016/0022-1694(83)90181-6Sadok, W., Lopez, J. R., & Smith, K. P. (2021). Transpiration increases under high-temperature stress: Potential mechanisms, trade-offs and prospects for crop resilience in a warming world. *Plant, Cell & Environment*, *44*(7), 2102–2116. https://doi.org/10.1111/pce.13970Scanlon, T. M., & Kustas, W. P. (2010). Partitioning carbon dioxide and water vapor fluxes using correlation analysis. *Agricultural and Forest Meteorology*, *150*(1), 89–99. https://doi.org/10.1016/J.AGRFORMET.2009.09.005Scanlon, T. M., & Kustas, W. P. (2012). Partitioning Evapotranspiration Using an Eddy Covariance-Based Technique: Improved Assessment of Soil Moisture and Land–Atmosphere Exchange Dynamics. *Vadose Zone Journal*, *11*(3). https://doi.org/10.2136/vzj2012.0025Scanlon, T. M., & Sahu, P. (2008). On the correlation structure of water vapor and carbon dioxide in the atmospheric

surface layer: A basis for flux partitioning. *Water Resources Research*, *44*(10), 10418–10418. https://doi.org/10.1029/2008WR006932Scanlon, T. M., Schmidt, D. F., & Skaggs, T. H. (2019). *Correlation-based flux partitioning of water vapor and carbon dioxide fluxes: Method simplification and estimation of canopy water use efficiency*. https://doi.org/10.1016/j.agrformet.2019.107732Schimel, D., Pavlick, R., Fisher, J. B., Asner, G. P., Saatchi, S., Townsend, P., Miller, C., Frankenberg, C., Hibbard, K., & Cox, P. (2015). Observing terrestrial ecosystems and the carbon cycle from space. *Global Change Biology*, *21*(5), 1762–1776. https://doi.org/10.1111/gcb.12822Schlesinger, W. H., & Jasechko, S. (2014). Transpiration in the global water cycle. *Agricultural and Forest Meteorology*, *189*, 115–117. https://doi.org/10.1016/j.agrformet.2014.01.011Schneider, J., Groh, J., Pütz, T., Helmig, R., Rothfuss, Y., Vereecken, H., & Vanderborght, J. (2021). Prediction of soil evaporation measured with weighable lysimeters using the FAO Penman–Monteith method in combination with Richards' equation. *Vadose Zone Journal*, *20*(1), e20102. https://doi.org/10.1002/vzj2.20102Skaggs, T. H., Anderson, R. G., Alfieri, J. G., Scanlon, T. M., & Kustas, W. P. (2018). *Fluxpart: Open source software for partitioning carbon dioxide and water vapor fluxes*. http://www.elsevier.com/open-access/userlicense/1.0/Stoy, P. C., El-Madany, T. S., Fisher, J. B., Gentine, P., Gerken, T., Good, S. P., Klosterhalfen, A., Liu, S., Miralles, D. G., Perez-Priego, O., Rigden, A. J., Skaggs, T. H., Wohlfahrt, G., Anderson, R. G., Coenders-Gerrits, A. M. J., Jung, M., Maes, W. H., Mammarella, I., Mauder, M., … Wolf, S. (2019). Reviews and syntheses: Turning the challenges of partitioning ecosystem evaporation and transpiration into opportunities. *Biogeosciences*, *16*(19), 3747–3775. https://doi.org/10.5194/BG-16-3747-2019Stoy, P. C., Katul, G. G., Siqueira, M. B. S., Juang, J. Y., Novick, K. A., Uebelherr, J. M., & Oren, R. (2006). An evaluation of models for partitioning eddy covariance-measured net ecosystem exchange into photosynthesis and respiration. *Agricultural and Forest Meteorology*, *141*(1), 2–18. https://doi.org/10.1016/j.agrformet.2006.09.001Stoy, P. C., Mauder, M., Foken, T., Marcolla, B., Boegh, E., Ibrom, A., Arain, M. A., Arneth, A., Aurela, M., Bernhofer, C., Cescatti, A., Dellwik, E., Duce, P., Gianelle, D., van Gorsel, E., Kiely, G., Knohl, A., Margolis, H., McCaughey, H., … Varlagin, A. (2013). A data-driven analysis of energy balance closure across FLUXNET research sites: The role of landscape scale heterogeneity. *Agricultural and Forest Meteorology*, *171–172*, 137–152. https://doi.org/10.1016/j.agrformet.2012.11.004Sulman, B. N., Moore, J. A. M., Abramoff, R., Averill, C., Kivlin, S., Georgiou, K., Sridhar, B., Hartman, M. D., Wang, G., Wieder, W. R., Bradford, M. A., Luo, Y., Mayes, M. A., Morrison, E., Riley, W. J., Salazar, A., Schimel, J. P., Tang, J., & Classen, A. T. (2018). Multiple models and experiments underscore large uncertainty in soil carbon dynamics. *Biogeochemistry*, *141*(2), 109–123. https://doi.org/10.1007/S10533-018-0509-Z/TABLES/1Sulman, B. N., Roman, D. T., Scanlon, T. M., Wang, L., & Novick, K. A. (2016). Comparing methods for partitioning a decade of carbon dioxide and water vapor fluxes in a temperate forest. *Agricultural and Forest Meteorology*, *226–227*, 229–245. https://doi.org/10.1016/J.AGRFORMET.2016.06.002Sun, X., Onda, Y., Ot-

suki, K., Kato, H., Gomi, T., & Liu, X. (2017). Change in evapotranspiration partitioning after thinning in a Japanese cypress plantation. *Trees*, *31*(5), 1411–1421. https://doi.org/10.1007/s00468-017-1555-1Talsma, C. J., Good, S. P., Jimenez, C., Martens, B., Fisher, J. B., Miralles, D. G., Mccabe, M. F., & Purdy, A. J. (2018). *Partitioning of evapotranspiration in remote sensing-based models*. https://doi.org/10.1016/j.agrformet.2018.05.010Thomas, C., Martin, J. G., Goeckede, M., Siqueira, M. B., Foken, T., Law, B. E., Loescher, H. W., & Katul, G. (2008). Estimating daytime subcanopy respiration from conditional sampling methods applied to multi-scalar high frequency turbulence time series. *Agricultural and Forest Meteorology*, *148*(8), 1210–1229. https://doi.org/10.1016/j.agrformet.2008.03.002van der Kamp, G., & Hayashi, M. (2009). Groundwater-wetland ecosystem interaction in the semiarid glaciated plains of North America. *Hydrogeology Journal*, *17*(1), 203–214. https://doi.org/10.1007/s10040-008-0367-1Wagle, P., Skaggs, T. H., Gowda, P. H., Northup, B. K., & Neel, J. P. S. (2020). *Flux variance similarity-based partitioning of evapotranspiration over a rainfed alfalfa field using high frequency eddy covariance data*.Wang, L., Good, S. P., & Caylor, K. K. (2014). Global synthesis of vegetation control on evapotranspiration partitioning. *Geophysical Research Letters*, *41*(19), 6753–6757. https://doi.org/10.1002/2014GL061439Wang, R., Li, L., Gentine, P., Zhang, Y., Chen, J., Chen, X., Chen, L., Ning, L., Yuan, L., & Lü, G. (2022). Recent increase in the observation-derived land evapotranspiration due to global warming. *Environmental Research Letters*, *17*(2), 024020. https://doi.org/10.1088/1748-9326/ac4291Wang-Erlandsson, L., Van Der Ent, R. J., Gordon, L. J., & Savenije, H. H. G. (2014). Contrasting roles of interception and transpiration in the hydrological cycle—Part 1: Temporal characteristics over land. *Earth System Dynamics*, *5*(2), 441–469. https://doi.org/10.5194/ESD-5-441-2014Webb, E. K., Pearman, G. I., & Leuning, R. (1980). Correction of flux measurements for density effects due to heat and water vapour transfer. *Quarterly Journal of the Royal Meteorological Society*, *106*(447), 85–100. https://doi.org/10.1002/qj.49710644707Wei, Z., Yoshimura, K., Wang, L., Miralles, D. G., Jasechko, S., & Lee, X. (2017a). Revisiting the contribution of transpiration to global terrestrial evapotranspiration. *Geophysical Research Letters*, *44*(6), 2792–2801. https://doi.org/10.1002/2016GL072235Wei, Z., Yoshimura, K., Wang, L., Miralles, D. G., Jasechko, S., & Lee, X. (2017b). Revisiting the contribution of transpiration to global terrestrial evapotranspiration. *Geophysical Research Letters*, *44*(6), 2792–2801. https://doi.org/10.1002/2016GL072235Will, R. E., Wilson, S. M., Zou, C. B., & Hennessey, T. C. (2013). Increased vapor pressure deficit due to higher temperature leads to greater transpiration and faster mortality during drought for tree seedlings common to the forest–grassland ecotone. *New Phytologist*, *200*(2), 366–374. https://doi.org/10.1111/nph.12321Williams, C. A., Scanlon, T. M., Albertson, J. D., Williams, C. A., Albertson, J. D., & Scanlon, T. M. (2007). *Influence of surface heterogeneity on scalar dissimilarity in the roughness sublayer*. *122*, 149–165. https://doi.org/10.1007/s10546-006-9097-xWutzler, T., Lucas-Moffat, A., Migliavacca, M., Knauer, J., Sickel, K., Šigut,

L., Menzer, O., & Reichstein, M. (2018). Basic and extensible post-processing of eddy covariance flux data with REddyProc. *Biogeosciences*, *15*, 5015–5030. https://doi.org/10.5194/bg-15-5015-2018Xu, K., Metzger, S., & Desai, A. R. (2017). Upscaling tower-observed turbulent exchange at fine spatio-temporal resolution using environmental response functions. *Agricultural and Forest Meteorology*, *232*, 10–22. https://doi.org/10.1016/j.agrformet.2016.07.019Xue, B., Wang, G., Xiao, J., Tan, Q., Shrestha, S., Sun, W., & Liu, T. (2020). Global evapotranspiration hiatus explained by vegetation structural and physiological controls. *Ecological Engineering*, *158*, 106046–106046. https://doi.org/10.1016/J.ECOLENG.2020.106046Zahn, E., Bou-Zeid, E., Good, S. P., Katul, G. G., Thomas, C. K., Ghannam, K., Smith, J. A., Chamecki, M., Dias, N. L., Fuentes, J. D., Alfieri, J. G., Kwon, H., Caylor, K. K., Gao, Z., Soderberg, K., Bambach, N. E., Hipps, L. E., Prueger, J. H., & Kustas, W. P. (2022). Direct partitioning of eddy-covariance water and carbon dioxide fluxes into ground and plant components. *Agricultural and Forest Meteorology*, *315*, 108790–108790. https://doi.org/10.1016/J.AGRFORMET.2021.108790Zhang, K., Kimball, J. S., & Running, S. W. (2016). A review of remote sensing based actual evapotranspiration estimation. *WIREs Water*, *3*(6), 834–853. https://doi.org/10.1002/wat2.1168Zhang, X.-J., Tang, Q., Pan, M., & Tang, Y. (2014). A Long-Term Land Surface Hydrologic Fluxes and States Dataset for China. *Journal of Hydrometeorology*, *15*(5), 2067–2084. https://doi.org/10.1175/JHM-D-13-0170.1Zhou, S., Yu, B., Zhang, Y., Huang, Y., & Wang, G. (2016). Partitioning evapotranspiration based on the concept of underlying water use efficiency. *Water Resources Research*, *52*(2), 1160–1175. https://doi.org/10.1002/2015WR017766Zhu, Z., Sun, X., Wen, X., Zhou, Y., Tian, J., & Yuan, G. (2006). Study on the processing method of nighttime CO2 eddy covariance flux data in ChinaFLUX. *Science in China Series D: Earth Sciences*, *49*(S2), 36–46. https://doi.org/10.1007/s11430-006-8036-5

Table 1. All CHEESEHEAD19 eddy covariance sites with open-path infrared gas analyzers with site descriptions and characteristics.

Site Name	Vegetation	Ameriflux ID	Latitude (°N)	Longitude (°W)	Tower Height (m
NW1	Red pine	US-PFb	45.97200	-90.32317	32
NW2	Aspen	US-PFc	45.96773	-90.30878	12
NW3	Wetland (Tussock stream)	US-PFd	45.96892	-90.30103	3
NW4	Lake (S shore)	US-PFe	45.97930	-90.30042	32
NE1	Pine	US-PFg	45.97348	-90.27230	32
NE2	Pine and young larch	US-PFh	45.95573	-90.24060	32
NE3	Hardwood, pine understory	US-PFi	45.97490	-90.23273	32
NE4	Maple	US-PFj	45.96187	-90.22703	32
SW1	Aspen	US-PFk	45.91490	-90.34250	32
SW2	Aspen/birch	US-PFl	45.94090	-90.31773	25
SW3	Hardwood	US-PFm	45.92067	-90.30990	32
SW4	Hardwood	US-PFn	45.93922	-90.28232	32

SE2	Maple, pine understory	US-PFp	45.93652	-90.26408	32
SE3	Aspen	US-PFq	45.92715	-90.24750	32
SE4	Tussock wetland	US-PFr	45.92448	-90.24745	3
SE5	Aspen	US-PFs	45.93808	-90.23818	12
SE6	Pine, aspen understory	US-PFt	45.91973	-90.22883	32

Table 2: The likelihood of Fluxpart success by site and error codes for the cause of failure.

Site Name	Veg.	Percent Valid Partitioning	Missing data due to all data are NAN	Missing due to
NW1	pine	32.69%	21.13%	4.24%
NW2	aspen	14.86%	21.79%	8.49%
NW3	wetland	28.75%	35.5%	8.48%
NW4	pine	27.72%	15.49%	10.00%
NE1	pine	0%	41.81%	4.75%
NE2	pine	33.49%	25.48%	6.64%
NE3	hardwood	26.23%	35.84%	5.88%
NE4	maple	38.85%	23.90%	5.03%
SW1	aspen	33.19%	27.4%	5.79%
SW2	aspen	24.66%	18.75%	6.33%
SW3	hardwood	40.87%	18.75%	5.62%
SW4	hardwood	39.21%	27.69%	5.16%
SE2	hardwood	35.72%	24.31%	10.15%
SE3	aspen	30.57%	22.24%	5.24%
SE4	wetland	21.35%	39.85%	9.03%
SE5	aspen	17.89%	38.23%	8.81%
SE6	pine	40.10%	22.49%	5.50%